Food Hydrocolloids 128 (2022) 107562

Contents lists available at ScienceDirect

Food Hydrocolloids

journal homepage: www.elsevier.com/locate/foodhyd

# Greaseproof, hydrophobic, and biodegradable food packaging bioplastics from C6-fluorinated cellulose esters

Susana Guzman-Puyol [a,b,*], Giacomo Tedeschi [a], Luca Goldoni [c], José J. Benítez [d], Luca Ceseracciu [e], Andreas Koschella [f], Thomas Heinze [f], Athanassia Athanassiou [a], José A. Heredia-Guerrero [a,b,**]

[a] Smart Materials, Nanophysics, Istituto Italiano di Tecnologia, Via Morego, 30, Genova, 16163, Italy
[b] Instituto de Hortofruticultura Subtropical y Mediterránea "La Mayora", Universidad de Málaga-Consejo Superior de Investigaciones Científicas (IHSM, UMA-CSIC), Bulevar Louis Pasteur 49, 29010, Malaga, Spain
[c] Analitical Chemistry Lab, Istituto Italiano di Tecnologia, Via Morego, 30, Genova, 16163, Italy
[d] Instituto de Ciencia de Materiales de Sevilla, Centro Mixto CSIC-Universidad de Sevilla, Calle Americo Vespucio 49, Isla de la Cartuja, Sevilla, 41092, Spain
[e] Materials Characterization Facility, Istituto Italiano di Tecnologia, Via Morego, 30, Genova, 16163, Italy
[f] Friedrich Schiller University Jena, Institute for Organic Chemistry and Macromolecular Chemistry, Center of Excellence for Polysaccharide Research, Humboldtstraße 10, D-07743, Jena, Germany

ARTICLE INFO

*Keywords:*
Bio-based plastics
Cellulose
C6-fluorinated carboxylic acid
Greaseproof paper
Biodegradability

ABSTRACT

Tridecafluorononanoic acid (TFNA), a C6-fluorinated carboxylic acid, was esterified with cellulose at different molar ratios (0:1, 1:1, 2:1, and 3:1) in a trifluoroacetic acid (TFA):trifluoroacetic anhydride (TFAA):$CHCl_3$ (2:1:1, v:v:v) solvent mixture. Free-standing films were obtained for all formulations and are presented as alternatives to composites and blends of paper with fluorinated molecules. Mechanical properties were investigated by tensile tests, and a plasticizer effect of fluorinated chains was observed. Interestingly, the wettability of these new cellulose derivatives was similar or even better than other common cellulose derivatives and fluorinated polymers employed in food packaging. Hydrodynamic properties were also improved by addition of TFNA, resulting in materials with water vapor permeability values comparable to other cellulose-based food packaging materials. In addition, films with the higher amounts of TFNA showed the required oil resistance for papers used in food packaging applications, as determined by the Kit Test. Finally, the biodegradation of these C6-fluorinated cellulose esters, assessed by biological oxygen demand (BOD) in seawater, was higher than typical bio-based polymers used in food packaging. The bioplastic synthesized at a molar ratio 1:1 (TFNA:cellulose) showed excellent performances in terms of greaseproof, hydrophobicity, ductility, and biodegradability, representing a sustainable alternative to typical plastics used in food packaging.

## 1. Introduction

Petroleum-based plastics are the predominant materials for food packaging. In fact, of 368 million tons of plastics produced in 2019, the 40% was used to fabricate food packaging materials (PlasticsEurope, 2020). Petroleum-based plastics offer good physical properties, chemical inertness, easy processing, high versatility, and low weight together with very attractive production costs (Guzmán-Puyol, Heredia, Heredia-Guerrero, & Benítez, 2021). However, depletion of fossil sources, their fluctuating prices, sever environmental problems derived from the pollution of oil extraction, monomer synthesis, and plastic production, and the massive use of plastics is driving the food packaging industry towards more sustainable and renewable options, being cellulose a realistic alternative (Guzman-Puyol et al., 2015; Heredia-Guerrero et al., 2017; Klemm, Heublein, Fink, & Bohn, 2005).

Paper and paperboard are the two main cellulose-based materials for food packaging purposes. They present interesting features such as complete biodegradability, sustainability, printability, good strength,

* Corresponding author. Instituto de Hortofruticultura Subtropical y Mediterránea "La Mayora", Universidad de Málaga-Consejo Superior de Investigaciones Científicas (IHSM, UMA-CSIC), Bulevar Louis Pasteur 49, 29010, Malaga, Spain.
** Corresponding author. Smart Materials, Nanophysics, Istituto Italiano di Tecnologia, Via Morego, 30, Genova, 16163, Italy.
*E-mail addresses:* susana.guzman@csic.es (S. Guzman-Puyol), ja.heredia@csic.es (J.A. Heredia-Guerrero).

https://doi.org/10.1016/j.foodhyd.2022.107562
Received 1 July 2021; Received in revised form 29 January 2022; Accepted 31 January 2022
Available online 6 February 2022

and light weight (Guzman-Puyol et al., 2015, 2019; Siró & Plackett, 2010). For this reason, paper and paperboards represent more than 30% of the global food packaging (Deshwal, Narender, Panjagari, & Alam, 2019). On the other hand, plain paper is not suitable to protect food because of its poor barrier properties (Hubbe & Pruszynski, 2020). Several approaches have been pointed out to overcome this drawback. For example, a common industrial strategy consists of a beating process, *i.e.*, a long-period hydration of paper fibers followed by the application of pressure to reduce their porosity (Sakare, Bharimalla, Dhakane-Lad, & Patil, 2020). However, this methodology is highly energy and time consuming. Other procedures propose the use of fluorinated compounds due to their low surface energy and omniphobicity (Cunha & Gandini, 2010; Imae, 2003; Zahid, Heredia-Guerrero, Athanassiou, & Bayer, 2017). Such properties are of particular interest for the packaging of edible fats, oils and greasy foodstuff, that requires a suitable resistance, usually known in literature as greaseproof paper (Deshwal, Narender Panjagari, & Alam, 2019; Marsh & Bugusu, 2007). Typically, the fluorinated agent is applied to the surface of the paper or to the cellulose fiber slurry before the formation of the sheet (Hubbe & Pruszynski, 2020). However, the use of long chain fluorinated polymers with perfluorinated (where all H are substituted by F) side chains of C8 or longer has been limited to very few applications due to their persistence in the environment and bioaccumulation (Ellis, Mabury, Martin, & Muir, 2001; Guo, Resnick, Efimenko, Genzer, & De Simone, 2007; Krafft & Riess, 2015; Larsen et al., 2006; Lau, Butenhoff, & Rogers, 2004; Trier, Taxvig, Rosenmai, & Pedersen, 2017). In fact, perfluorooctanoic acid (PFOA), a common degradation compound of fluorinated long-chain molecules, can be found in soil and body waters, being the oceans its main reservoir (Wang, Cousins, Scheringer, Buck, & Hungerbühler, 2014). Moreover, PFOA has been indicated as a potential carcinogen (Guo, Resnick, Efimenko, Genzer, & DeSimone, 2007). Nevertheless, more recent studies about the biopersistance of fluorinated chemicals has highlighted that fluoropolymers having C6 or lower fluorinated side chains can degrade into environmentally safe substances with a rapid bio-elimination rate (Larsen et al., 2006; Li et al., 2015; Schutzius, Bayer, Tiwari, & Megaridis, 2011). In addition to the above mentioned methodologies, chemical modification of cellulose has also been used to improve its physical properties. These chemical reactions include esterification, etherification, etc. and achieve an hydrophobic behavior of the resultant cellulose derivatives (Belgacem & Gandini, 2008; Cunha, Freire, Silvestre, Neto, & Gandini, 2006; Cunha et al., 2007; Cunha & Gandini, 2010; Heinze & Liebert, 2001; Heinze, Liebert, Pfeiffer, & Hussain, 2003). In particular, the mixed anhydride system using a mixture of trifluoroacetic acid (TFA), trifluoroacetic acid anhydride (TFAA), and chloroform has been employed to prepare cellulose esters with saturated, unsaturated and polyhydroxylated fatty acids, and multi-branched fluorinated carboxylic acid among others (Heredia-Guerrero et al., 2017; Tedeschi et al., 2018; Tedeschi et al., 2021). Non-fluorinated cellulose esters with chain length of fatty substituent >6, usually known as long-chain cellulose esters (LCCE), represent a class of commercially important polymers mainly due to the increase of the temperature window between melt flow and thermal decomposition

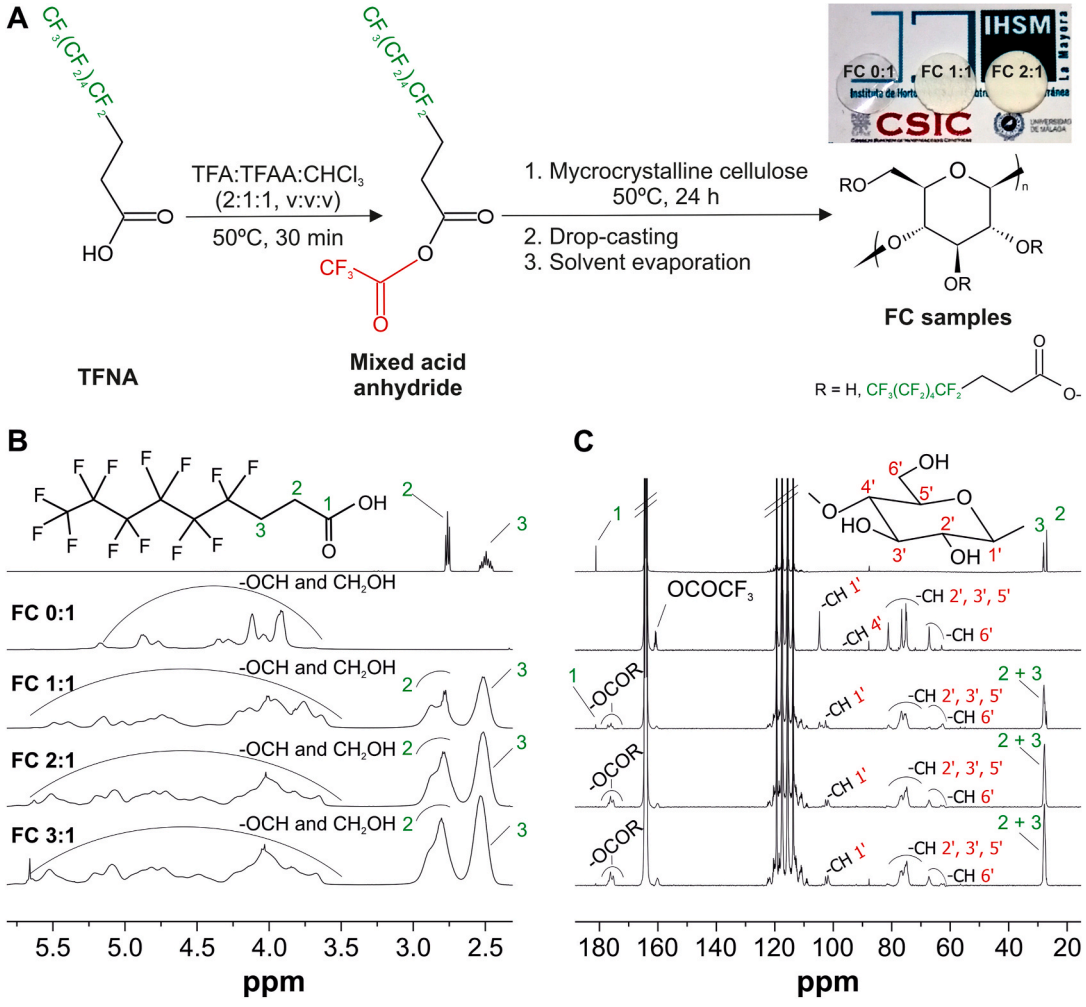


**Fig. 1.** **A**, scheme of the acylation of cellulose with TFNA and visual aspect of FC 0:1, 1:1, and 2:1 samples. **B–C**, $^{1}H$ and $^{13}C$ NMR spectra, respectively, in TFA-d of TFNA and FC 0:1, 1:1, 2:1, and 3:1 samples. The numbered chemical structures and main assignments of TFNA and cellulose are included.

with respect to short chain cellulose esters such as cellulose acetate or propionate. As a result, LCCEs present a better processability by extrusion (Edgar et al., 2001; Heinze, Liebert, & Koschella, 2006, p. 232; Tanaka, Iwata, & Iji, 2017). Moreover, in LCCEs, long-chain substitutes act as internal plasticizers, minimizing the risks of exudation and volatilization typical of classical external additives (Willberg-Keyriläinen, Vartiainen, Harlin, & Ropponen, 2017). However, unlike other common synthetic barrier polymers such as polypropylene (PP), oriented polypropylene (OPP), and polychlorotrifluoroethylene (PCTFE), LCCEs show an inverse relationship between their water vapor and oxygen barrier properties, which limits their full use in food packaging materials (Bras, Vaca-Garcia, Borredon, & Glasser, 2007). As shown in Fig. 1A for tridecafluorononanoic acid (TFNA), TFAA reacts with the carboxyl group to generate a reactive mixed anhydride that can be easily attacked by nucleophilic cellulose hydroxyl groups to generate ester groups. The presence of $CHCl_3$ in the solvent mixture is associated with higher degrees of substitution (Huang, 2012), while TFA is capable of dissolving cellulose by trifluoacetylation. Indeed, the fabrication of cellulose and cellulose-rich bioplastics and blends by TFA solubilization has been described several times (Guzman-Puyol et al., 2015, 2017, 2019; Bayer et al., 2014; Caligiuri et al., 2020; Papadopoulou et al., 2017; Tedeschi et al., 2020; Tran et al., 2016).

In this work, we report the fabrication of new hydrophobic, grease-proof, and biodegradable food packaging materials by chemical reaction of cellulose and a linear C-6 fluorinated monomer such as tridecafluorononanoic acid (TFNA) at different molar ratios using a mixture of TFA:TFAA:$CHCl_3$ as a common solvent. The corresponding cellulose esters were chemically characterized by NMR and ATR-FTIR spectroscopies. The effect of the degree of substitution on the mechanical properties, wettability, water uptake, grease resistance, and biodegradability were investigated and compared to those of common plastics used in food packaging.

## 2. Materials and methods

### 2.1. Materials

Chloroform, methanol, toluene, castor oil, heptane, trifluoroacetic acid (TFA), trifluoroacetic anhydride (TFAA), microcrystalline cellulose (MCC) from cotton linters (crystallinity ~79%), and tridecafluorononanoic acid (TFNA) were purchased from Sigma-Aldrich and used without additional purifications. Extra-virgin olive oil was purchased from a local market.

### 2.2. Synthesis of cellulose tridecafluorononanoate esters

The synthesis of cellulose tridecafluorononanoate esters (labeled as FC samples) was carried out as summarized in Fig. 1A. For this, different quantities of TFNA (0, 908, 1815, and 2723 mg) were dissolved in 25 mL of TFA:TFAA:$CHCl_3$ (2:1:1, v:v:v) in a 50 mL closed bottle and stirred for 30 min. Then, microcrystalline cellulose (375 mg) was added to each TFNA solution and stirred at 50 °C for 24 h. After reaction, solutions were cast into glass petri dishes and left in an aspirated hood at ~23 °C and ~50% RH until solvents were completely evaporated. Free-standing films were obtained and they were washed three times with methanol in order to remove any residual TFNA monomer. After washing, solvent was allowed to evaporate overnight and samples were stabilized at ~23 °C and ~44% RH for 7 days before analysis. The average film thickness was ~80 μm.

Table 1 summarizes the labeling and the composition of the different FC samples prepared in this work.

### 2.3. Morphological characterization

The morphology of the cellulose ester films was characterized by scanning electron microscopy (SEM), using a JEOL JSM-6490LA microscope working in high vacuum mode, with an acceleration voltage of 15 kV. Samples were previously covered with a ~10 nm gold coating by using a JEOL ION SPUTTER JFC 1100.

**Table 1**
Label, moles, mole fraction, and weight percentage of TFNA and cellulose of the different samples.

| Label | FC 0:1 | FC 1:1 | FC 2:1 | FC 3:1 |
|---|---|---|---|---|
| Moles of TFNA | 0 | 1 | 2 | 3 |
| Moles of anhydroglucose units | 1 | 1 | 1 | 1 |
| Mole fraction of TFNA | 0 | 0.5 | 0.67 | 0.75 |
| Mole fraction of cellulose | 1 | 0.5 | 0.33 | 0.25 |
| wt. % of TFNA | 0 | 71 | 83 | 88 |
| wt. % of cellulose | 100 | 29 | 17 | 12 |

Atomic force microscope (AFM) images were acquired with a Nanotec microscope (Natotec, Spain) equipped with a 10 × 10 $\mu m^2$ scanner. Aluminum back-coated silicon non-contact levers (Tap300Al-G, BudgetSensors, Bulgaria) with a nominal k value of 40 N/m and a tip curvature radius <10 nm were used. The lever was oscillated at its resonance frequency (~275 KHz) and the feedback set point was stablished around 75% of the free oscillating amplitude. Scanning speed was 1 line/s with a resolution of 500 x 500 points. Image reproducibility was checked by analyzing 3–5 regions of each sample at the maximum scanner range. At least, two samples per preparation were measured. Scanner calibration was performed with X, Y, and Z gratings (Mikro-Masch, Bulgaria) and images were processed and analyzed with the WSxM (Nanotec, Spain) program (Horcas et al., 2007).

### 2.4. Chemical characterization

Infrared spectra were obtained with an Attenuated Total Reflectance (ATR) accessory (MIRacle ATR, PIKE Technologies) coupled to a Fourier Transform Infrared (FTIR) spectrometer (Equinox 70 FT-IR, Bruker). All spectra were recorded in the range from 3800 to 600 $cm^{-1}$ with a resolution of 4 $cm^{-1}$, accumulating 128 scans. The H-bond energy, $E_H$, was calculated from ATR-FTIR data as follows (Ciolacu, Oprea, Anghel, Cazacu, & Cazacu, 2012):

$$E_H = \frac{1}{k} \cdot \frac{(\upsilon_0 - \upsilon)}{\upsilon_0} \quad (1)$$

where k is a constant with a value of 1.68 × $10^{-2}$ $kcal^{-1}$, $\nu_0$ is the standard wavenumber of the OH stretching mode ascribed to hydroxyl groups that do not interact by H-bonds (3600 $cm^{-1}$), and $\nu$ is the experimental wavenumber of samples.

For nuclear magnetic resonance (NMR) characterization, 10 mg of FC samples were dissolved in 1 mL of TFA-d (deuterated trifluoroacetic acid). Then, 500 μL of solution was transferred into 5 mm disposable tubes. All experiments were acquired on a Bruker Avance III 600 MHz spectrometer, equipped with 5 mm QCI cryoprobe and z shielded pulsed-field gradient coil. Temperature was actively monitored at 298K inside the probe and routines of automatic wobbling and shimming were run on each sample tube. In the $^1H$ NMR experiment, 128 transients were accumulated after applying a 30-degree pulse, with 65536 of digitalization points, a relaxation delay of 5s, over a spectral width of 25 ppm (offset at 6.18 ppm), with a fixed receiver gain (10). The phase of spectra was manually adjusted whereas baseline was automatically corrected. In the $^{13}C$ NMR spectrum, 5120 transients were accumulated after applying a 30-degree pulse, with 32768 of digitalization points, a relaxation delay of 2s, over a spectral width of 239 ppm (offset 100 ppm). An apodization exponential function equivalent to 1 and 5Hz were applied to the $^1H$ and $^{13}C$ FIDs respectively, before the Fourier transform. All spectra were referred to the not deuterated residual TFA solvent peak at 11.50 ppm for $^1H$ and 116.6 ppm for $^{13}C$, respectively.

Size Exclusion Chromatography (SEC) was used to determine molecular weight and molecular weight distribution of FC samples. A SEC

system from Agilent was used, which consists of a degasser, pump, autosampler, column oven, and a refractive index detector. FC 0:1 was carbanilated according to the protocol published elsewhere (Potthast et al., 2015). Tetrahydrofuran was used as eluent at 30 °C as well as column SDV lin M including guard column from Polymer Standards Service GmbH (PSS, Mainz, Germany). Calibration of the elution curves was based on polystyrene standards. For FC 2:1, *N,N*-dimethylacetamide containing 0.21% LiCl was used as an eluent at 30 °C. Columns GRAM guard/30/100 Å were purchased from PSS (Mainz, Germany). Calibration of the elution curves was based on poly(ethylene glycol) standards. Molar mass distribution curves were normalized to the molar mass of the nonfunctionalized repeating unit in order to compensate the influence of the substituent and its degree of substitution on the molar mass.

The crystallinity of FC films was analyzed by X-ray diffraction (XRD) using a Rigaku SmartLab X-Ray Diffractometer equipped with a copper rotating anode. The X-ray source was operated at 40 kV and 150 mA. A Gobel mirror was used to obtain a parallel beam and to suppress Cu Kβ radiation (1.392 Å). The measurements were performed using a $2\theta$ scan.

### 2.5. Mechanical characterization

Mechanical properties of the films were measured by uniaxial tensile tests on a dual column Instron 3365 universal testing machine. Dog-bone shaped samples were stretched at a rate of 5 mm/min. All stress-strain curves were recorded at 25 °C and 44% RH. Young's modulus, yield stress, and elongation at break values were calculated from the stress-strain curves. Ten measurements were conducted for each sample and the results were averaged to obtain a mean value.

### 2.6. Wettability, hydrodynamic characterization, and barrier properties

Static water and oil contact angle measurements were performed by using the sessile drop method in a DataPhysics OCAH 200 contact angle goniometer equipped with a CCD camera and image processing software operating under laboratory conditions (temperature 22–25 °C and relative humidity 50–60%). For the characterization, 5 μL droplets of MilliQ water for water contact angle and extra-virgin olive oil for oil contact angle were used. Up to 10 measurements were carried out on every sample at random locations and their average values and the corresponding standard deviations are reported.

Surface free energy was calculated from contact angle measurements based on the Owens, Wendt, Rabel & Kälble method (Owens & Wendt, 1969). This method presupposes that the surface tension of a liquid ($\gamma_l$) and the surface energy of a solid ($\gamma_s$) are the sum of a dispersive part ($\gamma^d$) and a non-dispersive one ($\gamma^{nd}$). The dispersive part includes dispersion interactions while the non-dispersive factor includes polar, hydrogen, and other van der Waals interactions. Based on the assumptions that the work of adhesion between a solid and a liquid is equal to a geometric mean of the work of cohesion of the solid and the work of cohesion of the liquid and combining with the Young's equation, it can be found the following formula:

$$2\sqrt{\gamma_s^{nd}\gamma_l^{nd}} + 2\sqrt{\gamma_s^{d}\gamma_l^{d}} = \gamma_l(1+cos\theta) \quad (2)$$

where ${\gamma_s}^{nd}$ is the non-dispersive component of solid surface energy, ${\gamma^{sd}}$ is the dispersive component of solid surface energy, ${\gamma_l}^{nd}$ is the non-dispersive component of liquid surface tension, ${\gamma_l}^{d}$ is the dispersive component of liquid surface tension, and $\theta$ is the static contact angle of the liquid on the solid. The measured contact angles of water and diiodomethane with surface tension components reported by Ström et al. (Ström, Fredriksson, & Stenius, 1987) were used to calculate the surface energy components.

For water uptake characterization, films were first dried by conditioning in a desiccator until no change in sample weight was measured. Dry samples were weighed (~30 mg) on a sensitive electronic balance (0.0001 g accuracy) and, then, placed in chambers at different relative humidities (0, 11, 57, 84 and 100% RH). Once the equilibrium was reached, each sample was weighed again and the amount of adsorbed water was calculated as the difference with the initial dry weight. Three measurements were taken and the results were averaged to obtain a mean value. Water uptake was calculated as indicated below:

$$Water\ uptake\ (\%) = \frac{m_f - m_0}{m_0} \cdot 100 \quad (3)$$

where $m_f$ is the sample weight at 11, 57, 84, or 100% RH and $m_0$ is the sample weight at 0% RH.

Water vapor transmission rate (WVTR) of FC samples was determined at 25 °C and under 100% relative humidity gradient (ΔRH %) according to the ASTM E96 standard method (Bedane, Eić, Farmahini-Farahani, & Xiao, 2015; Savadekar & Mhaske, 2012). 300 μL of deionized water (which generates 100% RH inside permeation cell) was placed in each test permeation cell with a 7 mm inside diameter and a 10 mm inner depth. FC samples were cut into circles and mounted on the top of permeation cells. The permeation cells were placed in 0% RH desiccator with anhydrous silica gel used as a desiccant agent. The water transferred through the film was determined from the weight change of the permeation cell every hour during 7 h using an electronic balance (0.0001 g accuracy). The weight loss of permeation cells was plotted as a function of time. The slope of each line was calculated by linear regression and the water vapor transmission rate (WVTR) was determined as below:

$$WVTR\ \left(g\ /\ \left(m^2 \cdot day\right)\right) = \frac{Slope}{Area\ of\ the\ film} \quad (4)$$

WVTR measurements were replicated three times for each sample and the results were averaged to obtain a mean value.

Oxygen permeation tests were performed by using an Oxysense 5250i device equipped with a film permeation chamber. Tests were conducted at room conditions (~25 °C, 50% RH) according to ASTM method F3136-15. The permeation chamber consisted of a cylinder with two parts: the sensing and the driving wells. The first one was equipped with an Oxydot fluorescence sensor sensible to oxygen gas. This chamber was purged with $N_2$ while the driving well was kept open to ambient conditions. Samples were cut as square pieces ($6 \times 6$ cm$^2$) and placed inside the chamber. The oxygen transmission rate (OTR) was measured by monitoring the oxygen uptake as a function of the time. At least ten repetitions were taken for each sample with coefficient of determination of ~0.995.

Grease resistance tests were carried out according the Tappi test method 559 cm-12, also named as the Kit Test (Li & Rabnawaz, 2018). This is a standard procedure to test the degree of oil repellency of paper and board sheets. The procedure applies different mixtures of castor oil, toluene, and heptane to a substrate for 15 s. Once the time is over, the fluid is cleaned with a tissue and the surface is examined by visual inspection. If a dark spot appears on the substrate, it means the oil has penetrated and the test has failed. The Kit Tests ranks from 1 to 12, being each point of the ranking related to a different combination of castor oil, toluene, and heptane (from viscous to fluid combinations of them). The Kit Test number is the highest test value with no dark spot on the sample. The higher the Kit Test number, better is the oil resistance of the sample. Ten measurements were performed for each sample and the results were averaged to obtain a mean value.

### 2.7. Biodegradation in seawater

Biodegradability was evaluated on selected FC samples by standard biochemical oxygen demand (BOD) tests that measure the oxygen consumption due to the bioactivity of microorganisms present in water (Emadian, Onay, & Demirel, 2017; Tosin, Weber, Siotto, Lott, & Innocenti, 2012). For each sample, three measurements were conducted, results averaged and the corresponding standard deviations calculated.

Carefully weighed samples (~200 mg) were finely minced and immersed in bottles with 164 mL of seawater collected from the Malaga (Spain) area shoreline. The oxygen consumed during the biodegradation was recorded for 30 days at 20 °C by using OxyTop®-i measuring heads (WTW, Germany). Seawater without any sample was used as a reference.

Weight loss after biodegradation tests were carried out by calculating the weight difference of the samples before and after immersion in seawater for a 30-days period. For this, ~200 mg were weighted in an electronic balance (0.0001 g accuracy). After degradation, the bottle content was passed through a 0.5 mm sieve and washed several times with MilliQ water. Then, samples were placed in a desiccator until water was completely removed and weighed again. The weight loss was calculated as difference relative to the dry weight. Three measurements were carried out for each sample and the results were averaged to obtain a mean value.

## 3. Results and discussion

### 3.1. Chemical and structural characterization

High-resolution $^{1}H$ and $^{13}C$ NMR were used to study the cellulose functionalization with TFNA, Fig. 1B and C. For TFNA, $^{1}H$ NMR showed fine signals of $CH_2$ in positions number 2 and 3 at 2.76 and 2.50 ppm, respectively. These fine structures were attributed to $J_{CH}$ and $J_{HF}$ coupling. After esterification of cellulose with TFNA, such structures returned unresolved broad peaks, similar to those of FC 0:1 as consequence of the reduction of $T_2$ time (the spin-spin relaxation time), characteristic of high molecular weight compounds such as polymers (Heredia-Guerrero et al., 2017). Regarding chemical shifts, no differences were observed for signal 3, being 2.50 ppm for TFNA and 2.52–2.53 ppm for FC derivatives. On the other hand, signals attributed to carbon 2 were found at 2.76 ppm for TFNA whereas for FC samples split into two peaks with chemical shifts in the range 2.67–3.01 ppm, overall shifting to low fields (high frequencies). This phenomenon was attributed to the formation of esters on different cellulose hydroxyl groups as previously reported (Heredia-Guerrero et al., 2017). Moreover, $^{13}C$ NMR was used to corroborate the formation of esters between cellulose and TFNA, Fig. 1C. TFNA presented a sharp CO peak resonance at 181.4 ppm, typical of acid groups, whose presence practically disappears in the C6-fluorinated cellulose esters. For the FC derivatives, this CO chemical shift appears as a set of broad peaks at 174.2–178.6 ppm, typical of CO ester groups, confirming the lack of regioselectivity of the reaction. Removal of TFNA monomers after washing with methanol was checked by two diagnostic signals of $^{13}C$ NMR. The first one, at ~26.9 ppm, ascribed to C2 of TFNA, and a second one at ~181 ppm, typical of the CO of acid groups. Both signals appeared clearly visible for TFNA monomer while for FC bioplastics, their intensities were negligible, confirming in this way the successful TFNA removal with methanol as previously described elsewhere (Heredia-Guerrero et al., 2017). From NMR spectra, the degree of substitution was inferred by calculation of the ratio between the integrated peak intensity of all cellulose $^{1}H$ signals from 3.45 to 6.71 ppm (7H) and the TFNA broad multiplet at 2.51 ppm (2H), normalizing the signal to the protons' number generating the corresponding peak. Table 2 shows the labeling, the theoretical degree of substitution and the degree of substitution calculated by NMR.

**Table 2**
Theoretical and experimental degree of substitution of FC 0:1, FC 1:1, FC 2:1 and FC 3:1 samples.

| Sample | Theoretical degree of substitution | Experimental degree of substitution |
|---|---|---|
| FC 0:1 | 0 | 0 |
| FC 1:1 | 1 | 0.95 |
| FC 2:1 | 2 | 1.32 |
| FC 3:1 | 3 | 1.36 |

For FC 1:1 sample, the degree of substitution was found to be similar to the theoretical one, while for FC 2:1 the experimental degree of substitution was lower than the one expected from the stoichiometric ratio. FC 3:1 showed an experimental degree of substitution very close to those of FC 2:1, suggesting that the esterification reaction did not further proceed despite the higher amount of the fluorinated carboxylic acid. Due to such slight difference in the degree of substitution, FC 3:1 was discarded and no more characterizations were performed for this molar ratio.

Size exclusion chromatography (SEC) was used to determine the molar mass and molar mass distribution of FC samples, Table 3. For FC 0:1, a number average molar mass ($M_n$) of ~17,000 g/mol was obtained and a number average degree of polymerization ($DP_n$) of 105. For FC 2:1, $M_n$ was found slightly lower (~11,600 g/mol) and the $DP_n$ decreased to 72. The SEC curves (Fig. S2) show a monomodal distribution for FC 0:1 whereas for FC 2:1 a shoulder at ~10,000 g/mol appears as a consequence of the higher amounts of reagents used during the reaction and the possibility of side reactions. Nevertheless, polymer degradation remains negligible by increasing the substitution as indicated by the almost constant polydispersity (Đ) value.

Fig. 2A shows the ATR-FTIR spectra of FC 0:1, 1:1, and 2:1 samples as well as pristine TFNA carboxylic acid. Main bands of FC 0:1 were associated with those of cellulose: O–H stretching mode at 3340 $cm^{-1}$, different C–H stretching modes at 2893 $cm^{-1}$, adsorbed water at 1651 $cm^{-1}$, and the C–O stretching mode at 1018 $cm^{-1}$ (Tedeschi et al., 2020). On the other hand, TFNA infrared spectrum displayed bands assigned to the C═O stretching mode of carboxylic acid groups at 1709 $cm^{-1}$, the C–H scissoring bending mode at 1444 $cm^{-1}$, and the asymmetrical and symmetrical $–CF_2-$ stretching mode at 1238 and 1140 $cm^{-1}$, respectively (Radaelli et al., 2016). FC 1:1 and 2:1 showed bands of both components with an intensity proportional to their presence in the corresponding cellulose ester. Interestingly, the band attributed to the C═O stretching mode was shifted to higher wavenumbers: 1736 $cm^{-1}$ for both FC 1:1 and 2:1 samples. This new position is indicative of ester groups, as previously determined by NMR. In addition, a shift to higher wavenumbers was also observed for the O–H stretching mode of FC samples, Fig. 2B. Thus, the $\nu$(O–H) wavenumber increased from 3340 $cm^{-1}$ for FC 0:1 to 3365 and 3404 $cm^{-1}$ for FC 1:1 and 2:1, respectively, Fig. 2B. Such a shift is indicative of less intense H-bonds, most likely due to the separation of cellulose polymer chains induced by TFNA chains (Tran et al., 2016). In fact, the calculated energy of the H-bond network was reduced, Fig. 2B.

Crystallinity of FC bioplastics was determined by XRD, Fig. S1. As previously reported for other cellulose-based bioplastics prepared in TFA, diffractograms present just a broad halo centered at 20° typical of amorphous polymers (Bayer et al., 2014; Guzman-Puyol et al., 2017).

### 3.2. Mechanical characterization

The mechanical properties of FC esters were determined by uniaxial tension tests, Fig. 3. Fig. 3A shows the typical stress-strain curves for FC 0:1, 1:1, and 2:1. FC 0:1 presented the typical behavior of cellulose films prepared by dissolving cellulose in TFA, with high values of Young's modulus and stress at break and poor elongation at break (Bayer et al., 2014; Guzman-Puyol et al., 2015, 2017). The curve of FC 1:1 showed a transition between brittle and ductile behavior, with relatively large modulus and strength in the initial portion (comparable to the unmodified material) of the curve, followed by large plastic deformation. Increasing the fluorinated content, Young's modulus values were

**Table 3**
Molar mass and polidispersity of FC 0:1 and FC 2:1 samples.

| Sample | $M_n$ (g/mol) | $M_w$ (g/mol) | Đ | $DP_n$ | $DP_w$ |
|---|---|---|---|---|---|
| FC 0:1 | 17,016 | 39,614 | 2.33 | 105 | 244 |
| FC 2:1 | 11,616 | 27,308 | 2.35 | 72 | 168 |

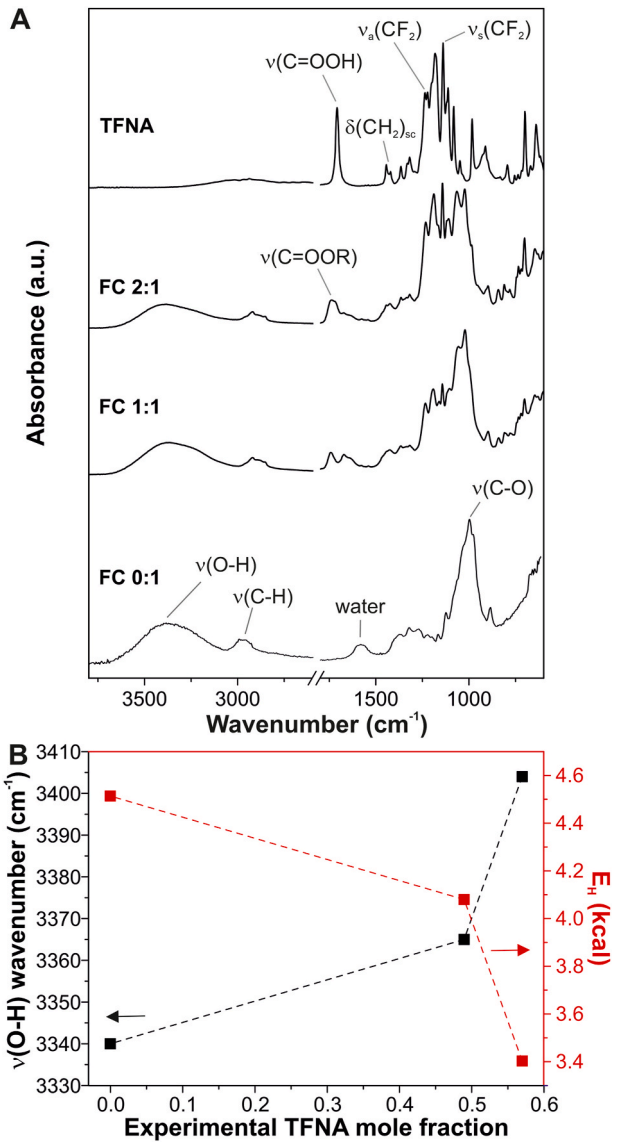


**Fig. 2.** **A**, ATR-FTIR spectra of the different FC samples and TFNA. Main assignments of both cellulose and TFNA are included. **B**, variation of the $\nu$(O–H) wavenumber and the energy of the H-bond network with the experimental TFNA mole fraction.

reduced drastically, while elongation at break was increasing, with final values ~25% for FC 2:1. These changes in the mechanical properties (from a rigid behavior for FC 0:1 to ductile materials in the case of FC 1:1 and FC 2:1) can be correlated with a plasticizer effect of fluorinated esters due to the intercalation of these kind of molecules between cellulose chains and the reduction (by –OH consumption during esterification) and weakness of the H-bond network (as observed by ATR-FTIR), which is strong enough for FC 1:1 to induce the build-up of stress at break during elastic deformation while allowing inter-chain sliding during plastic deformation. For FC 2:1, the lower strength of H-bonds network leads to plastic flow from low stress at break values (Guzman-Puyol et al., 2015). Top of Fig. 3B shows the Young's moduli of FC as a function of the experimental TFNA mole fraction (calculated from NMR data). FC 0:1 sample presented a Young's modulus of 1095 MPa, value in agreement with cellulose films prepared in the same conditions (Guzman-Puyol et al., 2017; Heredia-Guerrero et al., 2017). For FC 1:1 and 2:1, a dramatic decrease was observed with values of 281 and 4 MPa, respectively. To place the mechanical behavior of FC samples, a comparison of Young's modulus with those of other fluorinated and common polymers such as styrene-butadiene rubber (SBR), natural rubber, polychlorotrifluoroethylene (PCTFE), low density polyethylene (LDPE), ethylene-chlorotrifluoroethylene copolymer (ECTFE), polyperfluoroalkoxyethylene (PFA), fluoroethylene-propylene copolymer (FEP), polytetrafluoroethylene (PTFE), ethylene-tetrafluoroethylene copolymer (ETFE), high density polyethylene (HDPE), ethyl cellulose (EC), polyvinylidenefluoride (PVDF), cellulose acetate (CA), and carboxymethyl cellulose (CMC) was made, Fig. 3C (Brostow, 2007; Heredia-Guerrero et al., 2017; Teng, 2012). FC 2:1 was found similar to SBR and natural rubber. FC 1:1 presented a Young's modulus close to PFA and FEP, whereas FC 0:1 was located between HDPE and EC. It is remarkable that FC materials can cover a broad range of Young's modulus values, being in some cases close to rubbers or cellulose derivatives by modifying the experimental TFNA mole fraction.

On the other hand, an increase of strain at break values from ~3.3% for FC 0:1 to ~25.1 and ~25.6% for FC 1:1 and 2:1, respectively, was observed, Fig. 3B bottom. Finally, the relationship between stress at break and experimental TFNA mole fraction showed a strong decrease by increasing the mole fraction of TFNA from values of ~20 MPa for FC 0:1 to ~16 and ~1 MPa for FC 1:1 and 2:1, respectively.

### 3.3. Wettability, hydrodynamic characterization, and barrier properties

The wettability of FC specimens was investigated by determination of water and extra-virgin olive oil contact angles and the surface energy, Fig. 4. Fig. 4A shows the variation of water and extra-virgin olive oil contact angle with the experimental TFNA mole fraction. FC 0:1 presented a W-CA value of ~56°, typical of cellulose films obtained from evaporation of TFA solutions (Guzman-Puyol et al., 2015). Increasing the experimental TFNA mole fraction, samples exhibited higher water contact angles, as expected due to the increase of the fluorinated content. In particular, FC 1:1 showed a water contact angle of 107° whereas for FC 2:1 the value increased to 122°. When extra-virgin olive oil was used instead of water, a similar behavior was observed. FC 0:1 was oleophilic with an oil contact angle ~58°, while for FC 1:1 and 2:1 this value increased to 85 and 115°, respectively, comparable to other perfluoroacrylic polymer surfaces such as a perfluoroalkyl methacrylic copolymer (Steele, Bayer, & Loth, 2009). To check the possible influence of roughness on the wettability of FC samples, atomic force microscope (AFM) images were acquired, Fig. S3. As previously reported for other cellulose bioplastics prepared in TFA, an amorphous surface morphology was observed with no formation of crystalline regions (Bayer et al., 2014; Guzman-Puyol et al., 2019). From AFM images, the roughness average was calculated. FC 0:1 was the flattest sample with a roughness average of ~2.0 nm. Such a roughness was found to slightly increase with the experimental TFNA mole fraction, being ~3.9 nm for FC 1:1 and ~5.1 nm for FC 2:1. As demonstrated by the low roughness values, main differences in the wettability behavior of FC samples should be in the different chemical composition and not in the surface topographic modification during the esterification process. Moreover, oil resistance tests were conducted for all samples, inset Fig. 4A. FC 0:1 was the sample with the lowest oil resistance value (~3) as previously reported elsewhere (Tedeschi et al., 2020), increasing this number to ~6 for FC 1:1 and ~12 (the highest oil resistance) for FC 2:1. As described in literature, Kit Test number 5 represents the minimum safe oil resistance required for papers used in food packaging applications, thus demonstrating the possibility to use FC 1:1 and FC 2:1 samples for this kind of applications. To situate the hydrophobic character of FC samples, their water contact angles were compared with those of other cellulose derivatives and fluorinated polymers such as CMC, PVDF, EC, ECTFE, ETFE, FEP, PFA, and PTFE, Fig. 4B (Guzman-Puyol et al., 2015; Lee, Park, & Randall Lee, 2008; Song, Lee, Choi, & Kim, 2019). As expected, FC 0:1 contact angle was higher than carboxyl-rich polymer CMC. FC 1:1 was found in between of ECTFE and ETFE and much higher than a hydrophobic cellulose derivative such as ethyl cellulose. Finally, FC 2:1 was similar to PFA and PTFE. Total surface energies and their

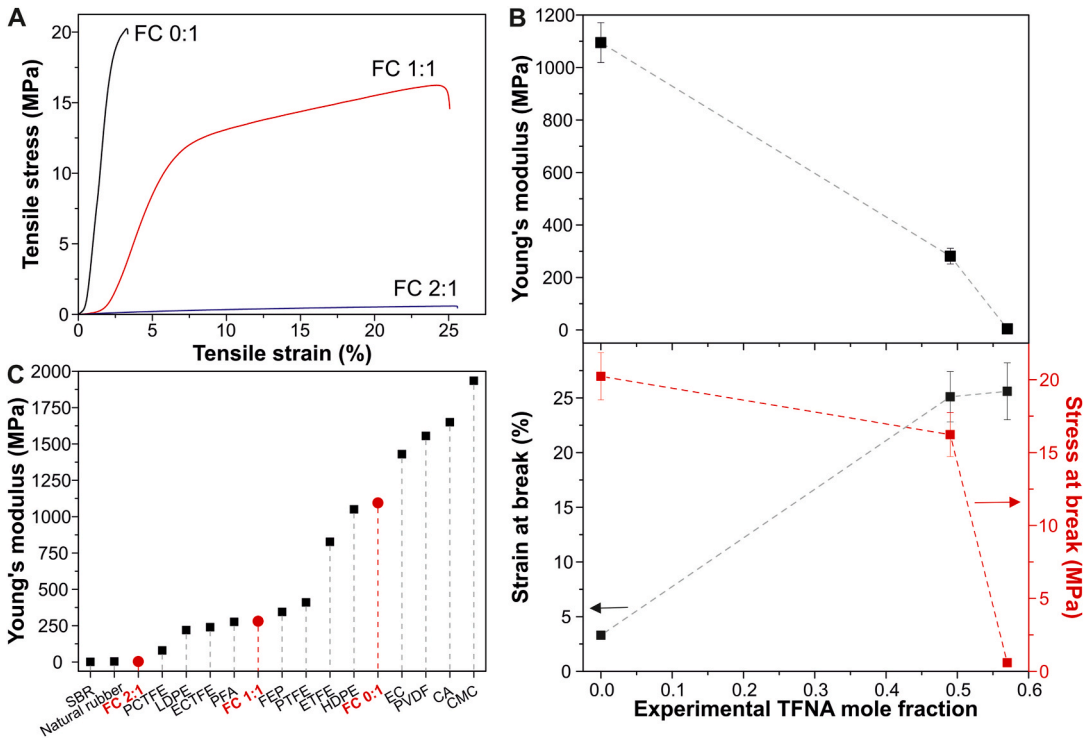


**Fig. 3.** **A**, typical stress-strain curves of FC samples. **B**, Young's modulus (top) and strain and stress at break (bottom) as a function of the experimental TFNA mole fraction. **C**, comparison of Young's modulus values of FC 0:1, 1:1, and 2:1 samples with other fluorinated and common polymers.

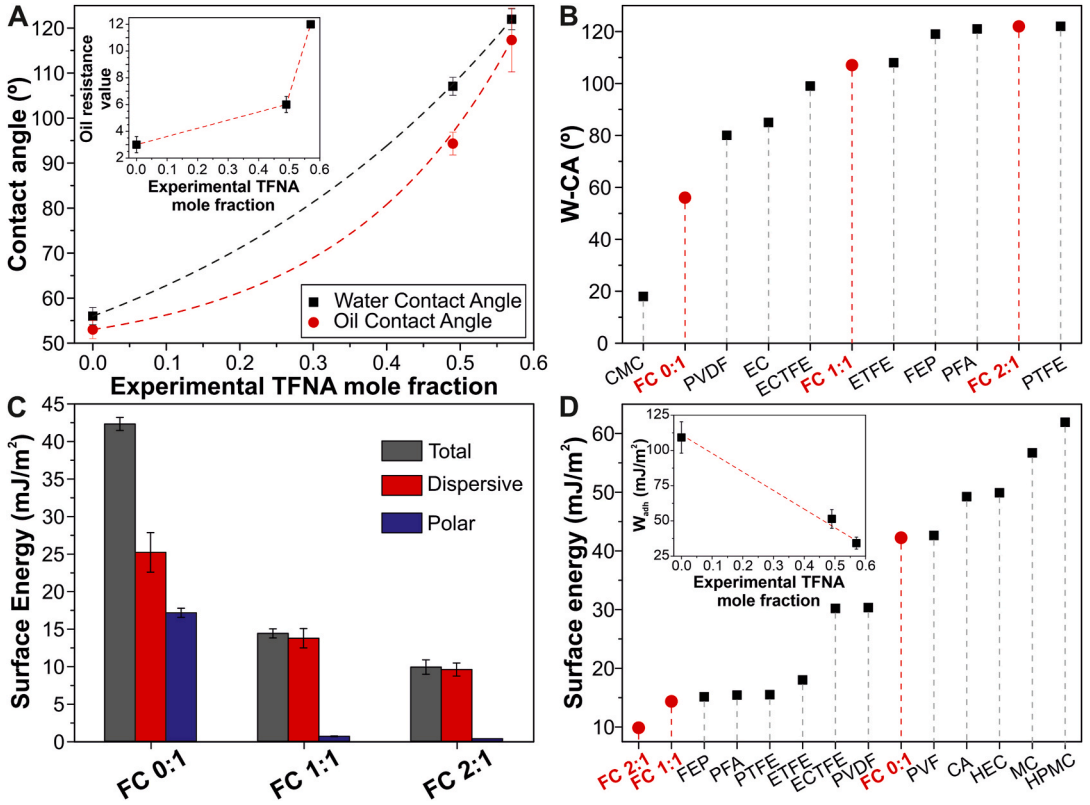


**Fig. 4.** **A**, water and oil contact angles as a function of experimental TFNA mole fraction. Inset: variation of the oil resistance value with the experimental TFNA mole fraction. **B**, comparison of water contact angles of FC samples and other common and fluorinated polymers. **C**, surface energies of FC 0:1, 1:1, and 2:1 samples. **D**, surface energy values of FC samples in comparison with other fluorinated polymers and cellulose derivatives. Inset: variation of the work of adhesion with the experimental TFNA mole fraction.

corresponding dispersive and polar contributions were also calculated for all FC samples, Fig. 4C. As observed, the surface energy decreased as the fluorinated content was higher, indicating a lower wettability. In particular, FC 0:1 was the sample with the highest surface energy (~42 $mJ/m^2$), decreasing to very low values of ~14 and ~10 $mJ/m^2$ for FC 1:1 and 2:1, respectively. The polar contribution was practically zero for FC 1:1 and 2:1 samples (~0.6 and 0.33 $mJ/m^2$, respectively) due to a lower exposure of hydroxyl groups by increasing the fluorinated content. The surface energies of FC samples were also compared to other fluorinated polymers and cellulose derivatives such as FEP, PFA, PTFE, ETFE, ECTFE, PVDF, polyvinylfluoride (PVF), CA, hydroxyethyl cellulose (HEC), methyl cellulose (MC), and hydroxypropyl methylcellulose (HPMC), Fig. 4D (Belov, Alentiev, Bogdanova, Vdovichenko, & Pashkevich, 2020; Białopiotrowicz & Jańczuk, 2002; Li et al., 2015; Mark, 2007; Shen, 2010). FC 1:1 and FC 2:1 presented the lowest values of surface energy, even lower than common fluorinated polymers such as FEP, PFA or PTFE. On the other hand, FC 0:1 showed a surface energy similar to PVF, but lower than other cellulose derivatives such as CA and MC. Finally, the work of adhesion, *i.e.* the work required to separate two phases (FC samples and water) from each other, was calculated from the water contact angle measurements, inset Fig. 4D. As observed, the work of adhesion was found to decrease by increasing the fluorinated content, being initially ~109 $mJ/m^2$ for FC 0:1 and decreasing to values ~51 and ~34 $mJ/m^2$ for FC 1:1 and 2:1 samples, respectively.

The moisture sorption isotherms of FC samples were characterized by determination of their water uptake at different relative humidities, Fig. 5A. Similar behaviors, denominated type II or sigmoidal isotherms, were observed for FC samples. On the one hand, FC 0:1 presented the typical behavior described for cellulose films (Guzman-Puyol et al., 2015), achieving final water uptakes of 30%. On the other hand, FC 1:1 and 2:1 samples presented lower water uptakes, due to the presence of fluorinated chains, reaching final water uptakes of ~7 and ~5%, respectively. The inset of Fig. 5A shows the water uptake at 100% RH as a function of the experimental TFNA mole fraction.

The water barrier properties of FC samples were tested by means of the water vapor transmission rate, Fig. 5B. In general, water permeability was reduced by increasing the experimental TFNA mole fraction, with values of ~8790 $g/m^2$day for FC 0:1, ~4375 $g/m^2$day for FC 1:1, and 2331 $g/m^2$day for FC 2:1. Such a decrease can be related to the reduction of hydroxyl groups consumed due to the condensation reaction to produce less polar ester groups and the presence of TFNA hydrophobic partially fluorinated chains that can effectively decrease the path of water molecules during the permeability process. A comparison of water permeability of FC samples with other papers such as paperboard, vegetable paper, wrap paper, and calendered paper typically used in food packaging is displayed in the inset of Fig. 5B (Ghosh, 2007; Tedeschi et al., 2020). FC 2:1 was found similar to vegetable (used for baking purposes) and wrap papers, whereas FC 1:1 showed a water permeability close to calendered paper. FC 0:1 displayed the highest water permeability value.

The oxygen barrier properties of FC samples were determined by measuring the oxygen transmission rate (OTR), Fig. 5B (bottom). OTR decreased exponentially by increasing the experimental TFNA mole fraction, being the values of ~315 $mL/m^2$day for FC 0:1, ~210 $mL/m^2$day for FC 1:1, and ~55 $mL/m^2$day for FC 2:1. Such a reduction can be explained by the hindered passage of oxygen molecules due to the insertion of fluorinated moieties. A comparison with other polymers commonly used for food packaging such as nylon 6, polylactic acid (PLA), polyvinyl chloride (PVC), polypropylene (PP), and LDPE is shown in the inset of Fig. 5B (Lu & Zheng, 2018; Peelman et al., 2013; J.; Wang et al., 2018). FC 2:1 showed the lowest OTR, with values similar to PLA and PVC, while FC 1:1 presented an OTR value similar to PP and FC 0:1 was the sample with the highest OTR, being similar to LDPE.

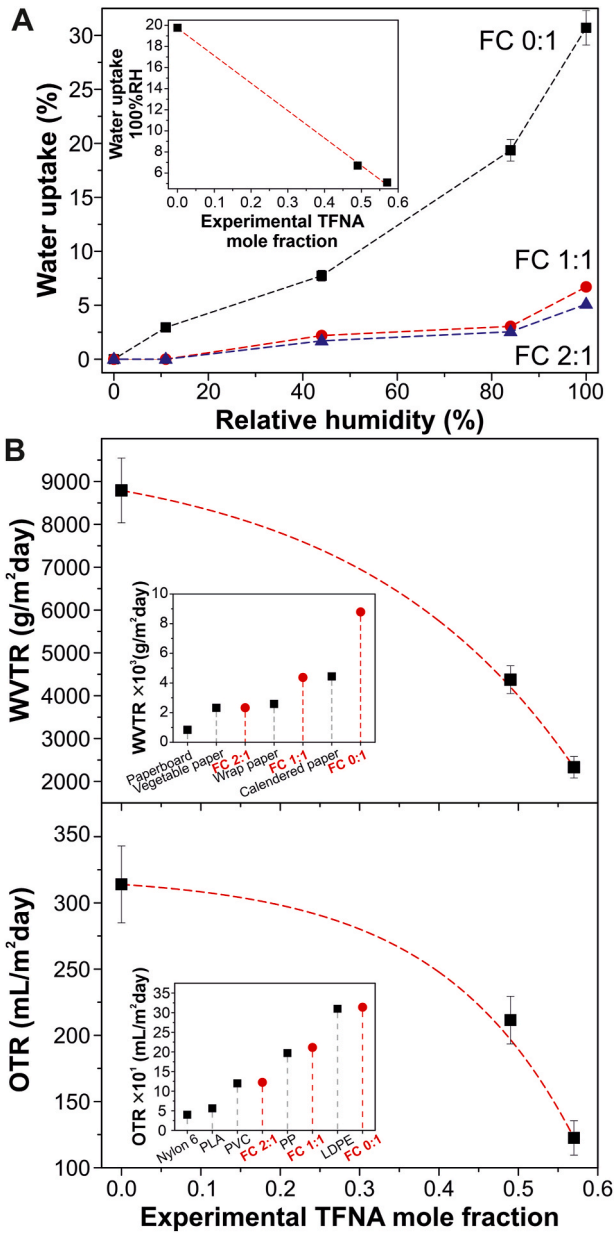


**Fig. 5. A**, water uptake of FC 0:1, 1:1, and 2:1 samples at different relative humidities. Inset: water uptake at 100% RH as a function of the experimental TFNA mole fraction. **B**, variation of water vapor (top) and oxygen (bottom) transmission rates with the experimental TFNA mole fraction. Insets: WVTR comparison of FC 0:1, 1:1, and 2:1 samples with other types of food packaging-grade papers (top) and OTR comparison of FC samples with other common polymers used in food packaging (bottom).

### 3.4. Biodegradation in seawater

The biodegradation of FC samples was tested by immersion of samples in seawater for a 30-day period, Fig. 6. Fig. 6A shows the biochemical oxygen demand (BOD) of FC samples. The highest biodegradability corresponded to FC 0:1, while as the fluorinated content increased, a reduction of the BOD was observed. Regarding the maximum BOD values, FC 0:1 presented a plateau at ~22 mg $O_2$/L after 4 days whereas the plateaus for FC 1:1 and 2:1 were observed at ~14 and 11 mg $O_2$/L, respectively, after ~18 days in both cases. Interestingly, for FC 0:1 and 1:1 biodegradation started immediately, while for FC 2:1 an initial, inactive period of 4 days was observed. A comparison of maximum BOD values of FC samples and other common polymers

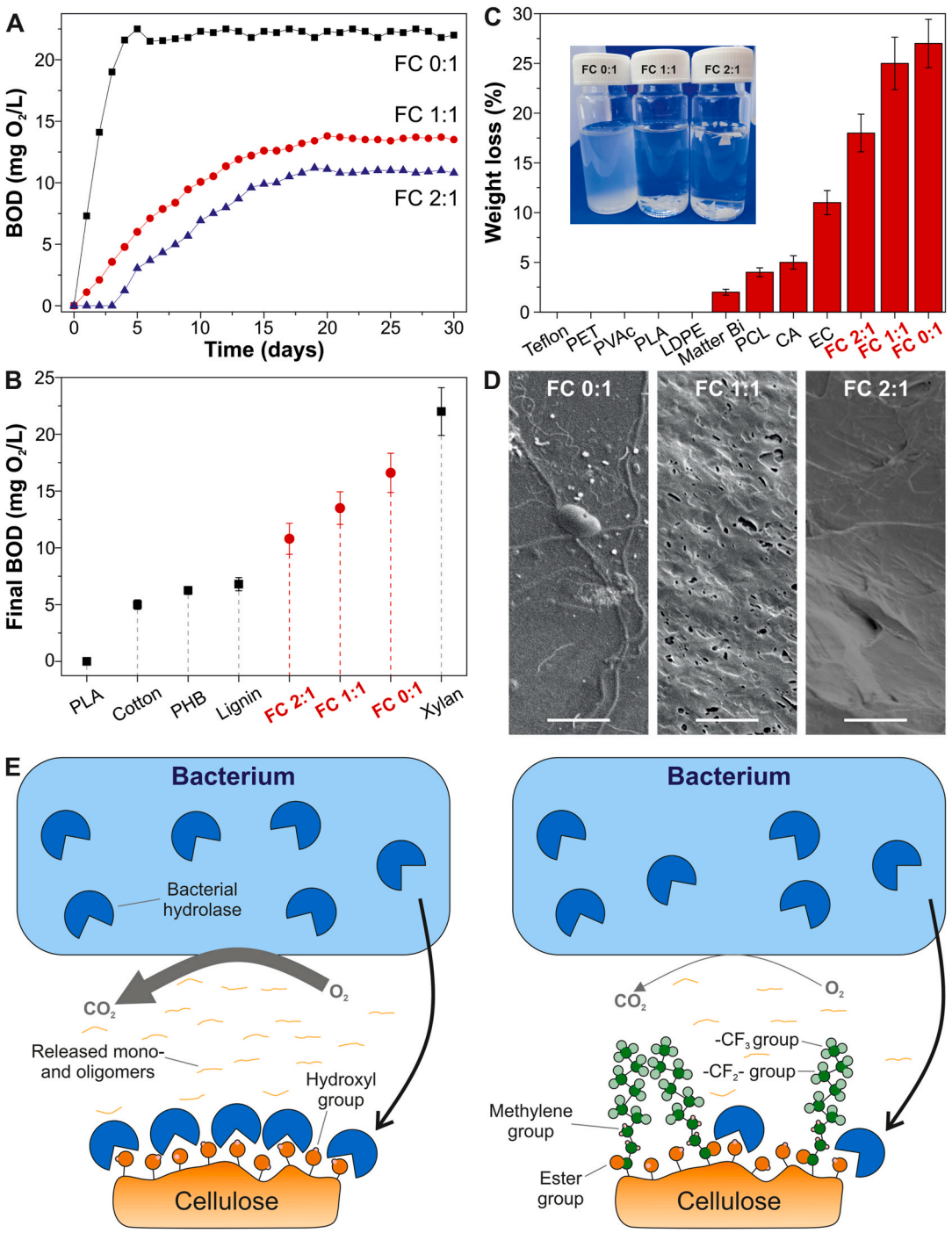


**Fig. 6.** **A**, biological oxygen demand (BOD) of FC 0:1, 1:1, and 2:1 samples. **B**, final BOD values of FC samples in comparison to other common bio-based polymers. **C**, weight loss of FC samples after the degradation process compared to other common man-made polymers. Inset: photograph of FC samples after the biodegradation process. **D**, top-view SEM images of FC samples after the BOD process. Scale bar: 10 μm. **E**, scheme representing the biodegradation in seawater of pure (FC 0:1) cellulose and C6-fluorinated cellulose esters (FC 1:1 and 2:1) by a generic bacterium.

such as PLA, cotton, polyhydroxybutyrate (PHB), lignin, and xylan is presented in Fig. 6B. FC samples were located between lignin and xylan, two common biopolymers considered biodegradable (Guzmán-Puyol et al., 2021; Jariyasakoolroj, Leelaphiwat, & Harnkarnsujarit, 2020; Maraveas, 2020). In comparison with other common bio-based polymers such as PLA and PHB, proposed as realistic substitutes of petroleum-based plastics (Bastioli, 2020; Maraveas, 2020), FC samples presented a higher biodegradation. A comparison of weight losses after BOD with Teflon, polyethylene terephthalate (PET), polyvinyl acetate (PVAc), PLA, LDPE, Matter Bi, polycaprolactone (PCL), CA, and EC was made and the results are shown in Fig. 6C. Teflon, PET, PVAc, PLA, and LDPE showed no weight loss, meaning a no biodegradation of these polymers in seawater after one month. When compared with other cellulose derivatives, FC samples presented higher weight losses than CA and EC, probably due to a lower degree of substitution and the amorphous character of cellulose samples prepared in TFA, Fig. S1 (Guzman-Puyol et al., 2015). The inset of Fig. 6C shows a photograph of vials containing FC samples after degradation. As observed, FC 0:1 turned into an opalescent solution with small fragments dispersed, whereas FC 1:1 and 2:1 presented clear solutions with pieces of the film dispersed.

SEM was performed on FC samples to characterize the surface erosion during biodegradation process, Fig. 6D. FC 0:1 was highly affected by bacteria colonizing the surface, while for FC 1:1 a clear wear with the occurrence of hollows and surface roughness was observed. FC 2:1 was less affected, showing a rough surface similar to those of sample before biodegradation test. Top-view SEM images of pristine FC samples are shown in Fig. S4. Finally, a scheme with a proposed biodegradation pathway for both non-fluorinated and fluorinated FC samples, based on the mechanisms for other biodegradable polymers (Nair, Sekhar, Nampoothiri, & Pandey, 2016; Polman, Gruter, Parsons, & Tietema, 2021; Sander, 2019), is represented in Fig. 6E. Cellulose, with a high number of free hydroxyl groups, can strongly interact with the enzymes released by the bacterial population from seawater. However, for TFNA-containing samples, fluorinated moieties can hinder the enzymatic attack, most likely due to the high hydrophobicity and the chemical inertness of fluorinated chains, partially avoiding the biodegradation process.

## 4. Conclusions

In this work, a C6-fluorinated carboxylic acid was esterified to cellulose by reaction in TFA:TFAA:$CHCl_3$ medium, as confirmed by NMR and ATR-FTIR. This is an alternative strategy to common simple addition of fluorinated compounds to paper for food packaging applications. The presence of fluorinated chains grafted to cellulose inferred plasticity, decreasing the Young's modulus and increasing the strain at break. In addition, the fluorinated chains improved the wettability, resulting in hydrophobic behaviors and very low surface energies, similar to common fluorinated polymers. Moreover, water uptake and water permeability were reduced by the fluorinated moieties with similar results to other papers used for food packaging. Furthermore, TFNA-containing samples showed very good biodegradation results, even better than current, commercial bio-based polymers launched to replace petroleum-based plastics. In view of all the above-mentioned properties, FC samples can be considered as potential alternative materials for food packaging uses, in particular for those where grease-proof, hydrophobic, and biodegradable properties are required.

## Notes

The authors declare no competing financial interest.

## Author statement

Conceptualization: S.G.-P., A.A., J.A.H.-G. Investigation: S.G.-P., G. T., L.G., J.J.B., L.C., A.K., T.H. Writing – Original Draft: S.G.-P., J.A.H.-G. Writing – Review & Editing: all authors. Supervision: J.A.H.-G. Funding acquisition: A.A.

## Declaration of competing interest

None.

## Acknowledgements

This work has been partially supported by the Spanish "Ministerio de Ciencia, Innovación y Universidades" project RYC2018-025079-I/AEI/10.13039/501100011033 (cofinanced by the European Social Fund, ESF) and by the Spanish Research Council (CSIC) project 202040E003.

## Appendix A. Supplementary data

Supplementary data to this article can be found online at https://doi.org/10.1016/j.foodhyd.2022.107562.

## References

Bastioli, C. (2020). Handbook of biodegradable polymers. In *Handbook of biodegradable polymers*. https://doi.org/10.1515/9781501511967

Bayer, I. S., Guzman-Puyol, S., Heredia-Guerrero, J. A., Ceseracciu, L., Pignatelli, F., Ruffilli, R., et al. (2014). Direct transformation of edible vegetable waste into bioplastics. *Macromolecules, 47*, 5135–5143. https://doi.org/10.1021/ma5008557

Bedane, A. H., Eić, M., Farmahini-Farahani, M., & Xiao, H. (2015). Water vapor transport properties of regenerated cellulose and nanofibrillated cellulose films. *Journal of Membrane Science, 493*, 46–57. https://doi.org/10.1016/j.memsci.2015.06.009

Belgacem, M. N., & Gandini, A. (2008). Surface modification of cellulose fibres. In *Monomers, polymers and composites from renewable resources*. https://doi.org/10.1016/B978-0-08-045316-3.00018-1

Belov, N. A., Alentiev, A. Y., Bogdanova, Y. G., Vdovichenko, A. Y., & Pashkevich, D. S. (2020). Direct fluorination as method of improvement of operational properties of polymeric materials. *Polymers, 12*. https://doi.org/10.3390/polym12122836

Białopiotrowicz, T., & Jańczuk, B. (2002). The wettability of a cellulose acetate membrane in the presence of bovine serum albumin. *Applied Surface Science, 201*(1–4). https://doi.org/10.1016/S0169-4332(02)00840-1

Bras, J., Vaca-Garcia, C., Borredon, M. E., & Glasser, W. (2007). Oxygen and water vapor permeability of fully substituted long chain cellulose esters (LCCE). *Cellulose, 14*(4). https://doi.org/10.1007/s10570-007-9123-2

Brostow, W. (2007). Mechanical properties. In *Physical properties of polymers handbook* (pp. 423–445). https://doi.org/10.1007/978-0-387-69002-5_24

Caligiuri, V., Tedeschi, G., Palei, M., Miscuglio, M., Martin-Garcia, B., Guzman-Puyol, S., et al. (2020). Biodegradable and insoluble cellulose photonic crystals and metasurfaces. *ACS Nano, 14*(8), 9502–9511. https://doi.org/10.1021/acsnano.0c03224

Ciolacu, D., Oprea, A. M., Anghel, N., Cazacu, G., & Cazacu, M. (2012). New cellulose-lignin hydrogels and their application in controlled release of polyphenols. *Materials Science and Engineering: C, 32*(3), 452–463. https://doi.org/10.1016/j.msec.2011.11.018

Cunha, A. G., Freire, C. S. R., Silvestre, A. J. D., Neto, C. P., & Gandini, A. (2006). Reversible hydrophobization and lipophobization of cellulose fibers via trifluoroacetylation. *Journal of Colloid and Interface Science, 301*(1), 333–336. https://doi.org/10.1016/J.JCIS.2006.04.078

Cunha, A. G., Freire, C. S. R., Silvestre, A. J. D., Neto, C. P., Gandini, A., Orblin, E., et al. (2007). Characterization and evaluation of the hydrolytic stability of trifluoroacetylated cellulose fibers. *Journal of Colloid and Interface Science, 316*(2), 360–366. https://doi.org/10.1016/J.JCIS.2007.09.002

Cunha, A. G., & Gandini, A. (2010). Turning polysaccharides into hydrophobic materials: A critical review. Part 1. Cellulose. *Cellulose, 17*(5), 875–889. https://doi.org/10.1007/s10570-010-9434-6

Deshwal, G. K., Narender Panjagari, R., & Alam, T. (2019). An overview of paper and paper based food packaging materials: Health safety and environmental concerns. *Journal of Food Science & Technology, 56*, 4391–4403. https://doi.org/10.1007/s13197-019-03950-z

Edgar, K. J., Buchanan, C. M., Debenham, J. S., Rundquist, P. A., Seiler, B. D., Shelton, M. C., et al. (2001). Advances in cellulose ester performance and application. *Progress in Polymer Science, 26*. https://doi.org/10.1016/S0079-6700(01)00027-2

Ellis, D. A., Mabury, S. A., Martin, J. W., & Muir, D. C. G. (2001). Thermolysis of fluoropolymers as a potential source of halogenated organic acids in the environment. *Nature, 412*(6844), 321–324. https://doi.org/10.1038/35085548

Emadian, S. M., Onay, T. T., & Demirel, B. (2017). Biodegradation of bioplastics in natural environments. *Waste Management, 59*, 526–536. https://doi.org/10.1016/j.wasman.2016.10.006

Ghosh, T. (2007). *WO2007131881A1-Use of a high performance water vapor barrier coating for paper under tropical conditions*.

Guo, J., Resnick, P., Efimenko, K., Genzer, J., & DeSimone, J. M. (2007). Alternative fluoropolymers to avoid the challenges associated with perfluorooctanoic acid. *Industrial & Engineering Chemistry Research, 47*(3), 502–508. https://doi.org/10.1021/ie0703179

Guzman-Puyol, S., Ceseracciu, L., Heredia-Guerrero, J. A., Anyfantis, G. C., Cingolani, R., Athanassiou, A., et al. (2015). Effect of trifluoroacetic acid on the properties of polyvinyl alcohol and polyvinyl alcohol–cellulose composites. *Chemical Engineering Journal, 277*, 242–251. https://doi.org/10.1016/J.CEJ.2015.04.092

Guzman-Puyol, S., Ceseracciu, L., Tedeschi, G., Marras, S., Scarpellini, A., Benítez, J. J., et al. (2019). Transparent and robust all-cellulose nanocomposite packaging materials prepared in a mixture of trifluoroacetic acid and trifluoroacetic anhydride. *Nanomaterials, 9*(3), 368. https://doi.org/10.3390/nano9030368

Guzman-Puyol, S., Russo, D., Penna, I., Ceseracciu, L., Palazon, F., Scarpellini, A., et al. (2017). Facile production of seaweed-based biomaterials with antioxidant and anti-inflammatory activities. *Algal Research, 27*, 1–11. https://doi.org/10.1016/j.algal.2017.08.015

Guzmán-Puyol, S., Heredia, A., Heredia-Guerrero, J. A., & Benítez, J. J. (2021). Cutin-inspired polymers and plant cuticle-like composites as sustainable food packaging materials. In *Sustainable food packaging technology* (pp. 161–198). https://doi.org/10.1002/9783527820078.ch6

Heinze, T., & Liebert, T. F. (2001). Unconventional methods in cellulose functionalization. *Progress in Polymer Science, 26*(9), 1689–1762. https://doi.org/10.1016/S0079-6700(01)00022-3

Heinze, T., Liebert, T., & Koschella, A. (2006). *Esterification of polysaccharides* (p. 232).

Heinze, T., Liebert, T. F., Pfeiffer, K. S., & Hussain, M. A. (2003). Unconventional cellulose esters: Synthesis, characterization and structure–property relations. *Cellulose, 10*(3), 283–296. https://doi.org/10.1023/A:1025117327970

Heredia-Guerrero, J. A., Goldoni, L., Benítez, J. J., Davis, A., Ceseracciu, L., Cingolani, R., et al. (2017). Cellulose-polyhydroxylated fatty acid ester-based bioplastics with tuning properties: Acylation via a mixed anhydride system. *Carbohydrate Polymers, 173*, 312–320. https://doi.org/10.1016/J.CARBPOL.2017.05.068

Horcas, I., Fernández, R., Gómez-Rodríguez, J. M., Colchero, J., Gómez-Herrero, J., & Baro, A. M. (2007). Wsxm: A software for scanning probe microscopy and a tool for nanotechnology. *Review of Scientific Instruments, 78*(1). https://doi.org/10.1063/1.2432410

Huang, F.-Y. (2012). Thermal properties and thermal degradation of cellulose tri-stearate (CTs). *Polymers, 4*. https://doi.org/10.3390/polym4021012

Hubbe, M. A., & Pruszynski, P. (2020). Greaseproof paper products: A review emphasizing ecofriendly approaches. *Bioresources, 15*(1). https://doi.org/10.15376/biores.15.1.1978-2004

Imae, T. (2003). Fluorinated polymers. *Current Opinion in Colloid & Interface Science, 8*(3), 307–314. https://doi.org/10.1016/S1359-0294(03)00050-5

Jariyasakoolroj, P., Leelaphiwat, P., & Harnkarnsujarit, N. (2020). Advances in research and development of bioplastic for food packaging. *Journal of the Science of Food and Agriculture, 100*. https://doi.org/10.1002/jsfa.9497

Klemm, D., Heublein, B., Fink, H.-P., & Bohn, A. (2005). Cellulose: Fascinating biopolymer and sustainable raw material. *Angewandte Chemie International Edition, 44*(22), 3358–3393. https://doi.org/10.1002/anie.200460587

Krafft, M. P., & Riess, J. G. (2015). Per- and polyfluorinated substances (PFASs): Environmental challenges. *Current Opinion in Colloid & Interface Science, 20*(3), 192–212. https://doi.org/10.1016/J.COCIS.2015.07.004

Larsen, B. S., Stchur, P., Szostek, B., Bachmura, S. F., Rowand, R. C., Prickett, K. B., et al. (2006). Method development for the determination of residual fluorotelomer raw materials and perfluorooctanoate in fluorotelomer-based products by gas chromatography and liquid chromatography mass spectrometry. *Journal of Chromatography A, 1110*(1–2), 117–124. https://doi.org/10.1016/J.CHROMA.2006.01.086

Lau, C., Butenhoff, J. L., & Rogers, J. M. (2004). The developmental toxicity of perfluoroalkyl acids and their derivatives. *Toxicology and Applied Pharmacology, 198*(2), 231–241. https://doi.org/10.1016/J.TAAP.2003.11.031

Lee, S., Park, J.-S., & Randall Lee, T. (2008). The wettability of fluoropolymer surfaces: influence of surface dipoles. *Langmuir, 24*(9), 4817–4826. https://doi.org/10.1021/la700902h

Li, S., Huang, J., Ge, M., Li, S. W., Xing, T., Chen, G., et al. (2015). Controlled grafting superhydrophobic cellulose surface with environmentally-friendly short fluoroalkyl chains by ATRP. *Materials and Design, 85*, 815–822. https://doi.org/10.1016/j.matdes.2015.07.083

Li, Z., & Rabnawaz, M. (2018). Oil- and water-resistant coatings for porous cellulosic substrates. *ACS Applied Polymer Materials, 1*(1), 103–111. https://doi.org/10.1021/acsapm.8b00106

Lu, Q. H., & Zheng, F. (2018). Polyimides for electronic applications. In *Advanced polyimide materials: Synthesis, characterization, and applications* (pp. 195–255). https://doi.org/10.1016/B978-0-12-812640-0.00005-6

Maraveas, C. (2020). Production of sustainable and biodegradable polymers from agricultural waste. *Polymers, 12*, 1127. https://doi.org/10.3390/POLYM12051127

Mark, J. (2007). *Physical properties of polymers handbook*. Springer. https://doi.org/10.1007/978-0-387-69002-5

Marsh, K., & Bugusu, B. (2007). Food packaging - roles, materials, and environmental issues: Scientific status summary. *Journal of Food Science, 72*, R39–R55. https://doi.org/10.1111/j.1750-3841.2007.00301.x

Nair, N. R., Sekhar, V. C., Nampoothiri, K. M., & Pandey, A. (2016). Biodegradation of biopolymers. In *Current developments in biotechnology and bioengineering: Production, isolation and purification of industrial products*. https://doi.org/10.1016/B978-0-444-63662-1.00032-4

Owens, D. K., & Wendt, R. C. (1969). Estimation of the surface free energy of polymers. *Journal of Applied Polymer Science, 13*(8), 1741–1747. https://doi.org/10.1002/app.1969.070130815

Papadopoulou, E. L., Heredia-Guerrero, J. A., Vázquez, M. I., Benavente, J., Athanassiou, A., & Bayer, I. S. (2017). Self-organized microporous cellulose-nylon membranes. *Polymer, 120*, 255–263. https://doi.org/10.1016/j.polymer.2017.06.002

Peelman, N., Ragaert, P., De Meulenaer, B., Adons, D., Peeters, R., Cardon, L., et al. (2013). Application of bioplastics for food packaging. *Trends in Food Science & Technology, 32*. https://doi.org/10.1016/j.tifs.2013.06.003

PlasticsEurope. (2020). *Plastics – the facts 2020. Brussels,. Plastics Europe*. Association of Plastics Manufacturers.

Polman, E. M. N., Gruter, G. J. M., Parsons, J. R., & Tietema, A. (2021). Comparison of the aerobic biodegradation of biopolymers and the corresponding bioplastics: A review. *The Science of the Total Environment, 753*, 141953. https://doi.org/10.1016/j.scitotenv.2020.141953

Potthast, A., Radosta, S., Saake, B., Lebioda, S., Heinze, T., Henniges, U., et al. (2015). Comparison testing of methods for gel permeation chromatography of cellulose: Coming closer to a standard protocol. *Cellulose, 22*(3), 1591–1613. https://doi.org/10.1007/S10570-015-0586-2/FIGURES/14

Radaelli, G., Heredia-Guerrero, J. A., Masood, M. T., Ceseracciu, L., Davis, A., Carzino, R., et al. (2016). Highly effective antiadhesive coatings from pH-modified water-dispersed perfluorinated acrylic copolymers: The case of vulcanizing rubber. *Advanced Materials Interfaces, 3*(13), 1600069. https://doi.org/10.1002/admi.201600069

Sakare, P., Bharimalla, A. K., Dhakane-Lad, J., & Patil, P. G. (2020). Development of greaseproof paper from banana pseudostem fiber for packaging of butter. *Journal of Natural Fibers, 18*, 1974–1982. https://doi.org/10.1080/15440478.2019.1710652

Sander, M. (2019). Biodegradation of polymeric mulch films in agricultural soils: Concepts, knowledge gaps, and future research directions. *Environmental Science and Technology, 53*. https://doi.org/10.1021/acs.est.8b05208

Savadekar, N. R., & Mhaske, S. T. (2012). Synthesis of nano cellulose fibers and effect on thermoplastics starch based films. *Carbohydrate Polymers, 89*(1), 146–151. https://doi.org/10.1016/j.carbpol.2012.02.063

Schutzius, M., Bayer, T. S., Tiwari, I. K., M, Megaridis, M., & C. (2011). Novel fluoropolymer blends for the fabrication of sprayable multifunctional superhydrophobic nanostructured composites. *Industrial & Engineering Chemistry Research, 50*(19), 11117–11123. https://doi.org/10.1021/ie200814r

Shen, Q. (2010). *Surface properties of cellulose and cellulose derivatives: A Review*. https://doi.org/10.1021/bk-2009-1019.ch012

Siró, I., & Plackett, D. (2010). Microfibrillated cellulose and new nanocomposite materials: A review. *Cellulose, 17*(3), 459–494. https://doi.org/10.1007/s10570-010-9405-y

Song, K., Lee, J., Choi, S.-O., & Kim, J. (2019). Interaction of surface energy components between solid and liquid on wettability, and its application to textile anti-wetting finish. *Polymers, 11*(3). https://doi.org/10.3390/polym11030498

Steele, A., Bayer, I., & Loth, E. (2009). Inherently superoleophobic nanocomposite coatings by Spray Atomization. *Nano Letters, 9*(1), 501–505. https://doi.org/10.1021/nl8037272

Ström, G., Fredriksson, M., & Stenius, P. (1987). Contact angles, work of adhesion, and interfacial tensions at a dissolving Hydrocarbon surface. *Journal of Colloid and Interface Science, 119*(2), 352–361. https://doi.org/10.1016/0021-9797(87)90280-3

Tanaka, S., Iwata, T., & Iji, M. (2017). Long/short chain mixed cellulose esters: Effects of long acyl chain structures on mechanical and thermal properties. *ACS Sustainable Chemistry & Engineering, 5*(2). https://doi.org/10.1021/acssuschemeng.6b02066

Tedeschi, G., Guzman-Puyol, S., Ceseracciu, L., Benitez, J. J., Goldoni, L., Koschella, A., Heinze, T., et al. (2021). Waterproof-breathable films from multi-branched fluorinated cellulose esters. *Carbohydrate Polymers, 271*, 118031. https://doi.org/10.1016/J.CARBPOL.2021.118031

Tedeschi, G., Guzman-Puyol, S., Ceseracciu, L., Paul, U., Picone, P., Di Carlo, M., et al. (2020). Multifunctional bioplastics inspired by wood composition: Effect of hydrolyzed lignin addition to xylan-cellulose matrices. *Biomacromolecules, 21*(2). https://doi.org/10.1021/acs.biomac.9b01569

Tedeschi, G., Guzman-Puyol, S., Paul, U., Barthel, M., Goldoni, L., Caputo, G., et al. (2018). Thermoplastic cellulose acetate oleate films with high barrier properties and ductile behaviour. *Chemical Engineering Journal, 348*. https://doi.org/10.1016/j.cej.2018.05.031

Teng, H. (2012). Overview of the development of the fluoropolymer industry. *Applied Sciences, 2*(2). https://doi.org/10.3390/app2020496

Tosin, M., Weber, M., Siotto, M., Lott, C., & Innocenti, F. D. (2012). Laboratory test methods to determine the degradation of plastics in marine environmental conditions. *Frontiers in Microbiology, 3*(JUN), 225. https://doi.org/10.3389/fmicb.2012.00225

Tran, T. N., Paul, U., Heredia-Guerrero, J. A., Liakos, I., Marras, S., Scarpellini, A., et al. (2016). Transparent and flexible amorphous cellulose-acrylic hybrids. *Chemical Engineering Journal, 287*, 196–204. https://doi.org/10.1016/j.cej.2015.10.114

Trier, X., Taxvig, C., Rosenmai, A. K., & Pedersen, G. A. (2017). PFAS in paper and board for food contact - options for risk management of poly- and perfluorinated substances. In *, 17. Nordic Council of ministers*.

Wang, Z., Cousins, I. T., Scheringer, M., Buck, R. C., & Hungerbühler, K. (2014). Global emission inventories for C4–C14 perfluoroalkyl carboxylic acid (PFCA) homologues from 1951 to 2030, Part I: Production and emissions from quantifiable sources. *Environment International, 70*, 62–75. https://doi.org/10.1016/J.ENVINT.2014.04.013

Wang, J., Gardner, D. J., Stark, N. M., Bousfield, D. W., Tajvidi, M., & Cai, Z. (2018). Moisture and oxygen barrier properties of cellulose nanomaterial-based films. *ACS Sustainable Chemistry & Engineering, 6*. https://doi.org/10.1021/acssuschemeng.7b03523

Willberg-Keyriläinen, P., Vartiainen, J., Harlin, A., & Ropponen, J. (2017). The effect of side-chain length of cellulose fatty acid esters on their thermal, barrier and mechanical properties. *Cellulose, 24*(2). https://doi.org/10.1007/s10570-016-1165-x

Zahid, M., Heredia-Guerrero, J. A., Athanassiou, A., & Bayer, I. S. (2017). Robust water repellent treatment for woven cotton fabrics with eco-friendly polymers. *Chemical Engineering Journal, 319*, 321–332. https://doi.org/10.1016/j.cej.2017.03.006